Int. J. Heat Mass Transfer. Vol. 28, No. 8, pp. 1469–1479, 1985
Printed in Great Britain

0017–9310/85 $3.00 + 0.00

The effect of the corrugation inclination angle on the thermohydraulic performance of plate heat exchangers

W. W. FOCKE,* J. ZACHARIADES and I. OLIVIER

Chemical Engineering Research Group, Council for Scientific and Industrial Research, PO Box 395, Pretoria 0001, Republic of South Africa

(*Received* 5 *September* 1984 *and in final form* 30 *January* 1985)

Abstract—It is well established that the inclination angle between plate corrugations and the overall flow direction is a major parameter in the thermohydraulic performance of plate heat exchangers. Application of an improved flow visualization technique has demonstrated that at angles up to about 80° the fluid flows mainly along the furrows on each plate. A secondary, swirling motion is imposed on the flow along a furrow when its path is crossed by streams flowing along furrows on the opposite wall. Through the use of the electrochemical mass transfer analogue, it is proved that this secondary motion determines the transfer process; as a consequence of this motion the transfer is fairly uniformly distributed across the width of the plates. The observed maximum transfer rate at an angle of about 80° is explained from the observed flow patterns. At higher angles the flow pattern becomes less effective for transfer; in particular at 90° marked flow separation is observed.

1. INTRODUCTION

THE CONVENTIONAL plate heat exchanger consists of a stack of corrugated metal plates clamped together in a frame. Each plate has four corner ports which, in pairs, provide access to the flow passages on either side of the plate. Sealing is accomplished with elastomeric gaskets so arranged that the two streams exchanging heat pass through alternate flow passages.

The embossed patterns provide a substantially larger surface area than flat plates, improve plate rigidity and provide a mechanical means of maintaining the channel gap. The corrugation geometry determines, to a great extent, the thermohydraulic performance of the exchanger. However, the information available on this aspect is mostly proprietory.

The corrugated patterns in general use are of chevron (herringbone) design; the labels are descriptive of the way in which the corrugations are arranged. Successive plates are assembled with the chevron patterns pointing in opposite directions, thereby producing a complex three-dimensional flow passage of almost constant cross-sectional flow area.

Previous investigations have shown that the angle at which the corrugations are placed relative to the main flow direction, is a major parameter influencing performance. However, these studies have either been limited to the effect of heat transfer [1, 2], have considered only a limited range of angles [3], or have given little information on the local flow patterns and their effect on transfer. Since both pressure drop and heat transfer are important design parameters, a more comprehensive study was called for.

The present investigation is limited to the effect of the corrugation inclination angle, β, on the heat transfer and pressure drop when the plates are corrugated sinusoidally. Experimental transfer data were obtained using an electrochemical mass transfer analogue. An attempt is made to explain the dependence on β of the observed transfer and pressure drop, in terms of observed flow patterns.

2. EXPERIMENTAL

2.1. *Technique*

The diffusion-limited current technique (DLCT) [4, 5] was used to evaluate heat transfer rates by analogy. The method is suitable for simulating constant wall-temperature heat transfer at high Prandtl numbers.

The theory of the DLCT is based on a diffusion-controlled reaction of an ion at the electrode–electrolyte interface. The solution conductivity is increased to the point where ionic migration of the reacting species becomes negligible, by adding large amounts of an 'inert' electrolyte. Limiting current conditions are indicated by a plateau region on a current–potential scan. Under these conditions, the surface concentration of the reacting species may be assumed to be zero and the mass transfer coefficient is then evaluated from

$$k = I_L/(zFCA_e). \quad (1)$$

The ferricyanide/ferrocyanide redox couple was chosen as the electrochemical system with potassium cabonate as the inert carrier electrolyte. The Stokes–Einstein ratio for this system [6] is:

$$D\eta/T = 2.29 \times 10^{-15}\ \text{kg m}^{-2}\ \text{s}^{-2}\ \text{K}^{-1}. \quad (2)$$

* Now at Dept. of Materials Science and Engineering, MIT, Cambridge, MA 02138, U.S.A.

NOMENCLATURE

A	cross-sectional free flow area [m^2]
A_d	developed surface area for heat transfer [m^2]
A_e	electrode area [m^2]
A_p	projected surface area for heat transfer [m^2]
B	constant, equation (A18)
C	concentration [mol m^{-3}]
c	constant, equation (A2)
D	diffusion coefficient [$m^2\ s^{-1}$]
d_e	equivalent diameter: twice average plate spacing [m]
d_h	hydraulic diameter: four times volume/A_d [m]
F	Faraday constant [C/eqv]
f	friction factor ($2\Delta P d_e/\rho u^2 L$)
I_L	limiting current [A]
j	Colburn j-factor, $Sh/(Re\ Sc^{1/2})$
K	geometric constant, equation (A1)
k	mass transfer coefficient [$m\ s^{-1}$]
L	length [m]
n	number of subchannels across channel width
p	corrugation pitch [m]
$P, \Delta P$	pressure, pressure drop [Pa]
q	flow rate [$m^3\ s^{-1}$]
Re	Reynolds number, ud_e/ν
s	average velocity gradient at wall [s^{-1}]
Sc	Schmidt number, ν/D
Sh	Sherwood number, kd_e/D
T	temperature [K]
u	local fluid velocity [$m\ s^{-1}$]
u	average fluid velocity [$m\ s^{-1}$]
W	plate width [m]
x, y	Cartesian coordinates [m]
z	charge number.

Greek symbols

β	corrugation inclination angle to main flow direction [rad]
η	dynamic viscosity [Pa s]
ν	kinematic viscosity. [$m^2\ s^{-1}$]

Subscripts

c	subchannel
1, 2	index subscripts referring to smaller and larger electrode segments, respectively.

This equation allows the estimation of the diffusion coefficient from viscosity measurements.

2.2. *Apparatus*

The experimental set-up is shown schematically in Fig. 1. The most important part was an acrylic cell with a test section into which test plates were fitted (see Fig. 2). The cell formed a rectangular channel with a low aspect ratio, having a width of 100 mm and a height of 10 mm. Wire mesh screens were used at the inlet to break up flow vortices. A converging section improved the velocity profile and reduced the turbulent intensity, while the inlet length of 600 mm allowed final flow development.

To simulate a single compartment in a plate heat exchanger the test plate surfaces were machined in the form of sinusoidal corrugations, of wave-length 10 mm and amplitude 2.5 mm, running the full width of the plate. Test plates were fitted into the test section with the corrugations abutting at an angle of 2β. The test plates were 100 mm wide and 440 mm long. The ends were chamfered to smooth the transition from the rectangular duct to the flow passage of the plate heat exchanger.

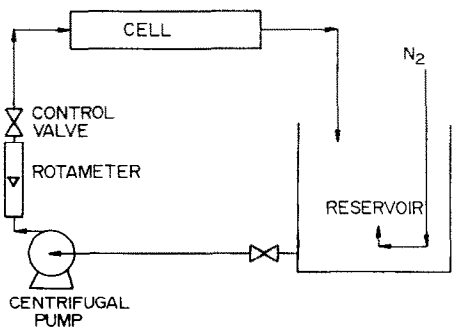

FIG. 1. Experimental set-up.

The test plates contained embedded nickel-plated brass electrodes. The cathode plates were divided into three electrode segments each 112 mm long, and the anode plates were continuous with their ridges constructed from an epoxy resin to prevent electrical contact between the electrodes. The use of opposing electrodes was essential to ensure limiting current conditions over the total length of the cathodes.

Plates with corrugation inclination angles of $\beta = 0°$, 30°, 45°, 60°, 72°, 80°, and 90° relative to the main flow direction were tested. The angles, $\beta = 72°$ and 80°, were chosen on the basis of the study by Rosenblad and Kullendorff [1], which indicated local extrema in the heat transfer for these angles. The resulting channels varied from a set of ten separate channels (sine-ducts) in parallel ($\beta = 0°$) to a single undulating channel of constant rectangular cross-section ($\beta = 90°$). In the latter case the corrugations of the two plates were in phase and therefore did not abut (see Fig. 7); the plate spacing was kept the same as in the other

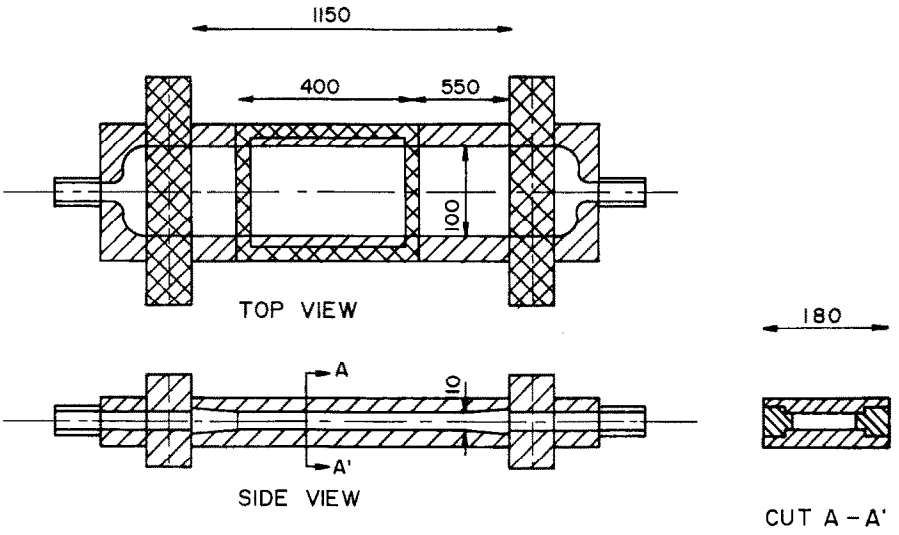

FIG. 2. Test cell.

configurations. Intermediate angles resulted in three-dimensional multiply-connected flow passages.

Flow rates were measured with a set of rotameters, and temperature to $\pm 0.1°C$ with precision mercury thermometers. Limiting currents were measured using a constant voltage supply and a digital multimeter.

Pressure drop was measured with a Gould DR3000 series differential pressure transmitter using distilled water as the medium. Pressure taps were located 100 mm upstream and 300 mm downstream of the test section. Corrections were made for the additional flowpath length and for entrance and exit losses. The corrections were based on measurements with a rectangular channel (flat plates with the same chamfer angle) of similar cross-sectional free flow area (0.5×10^{-3} m^2). The corrections ranged from a maximum of $\sim 12\%$ and $\sim 4\%$ for 30° and 45° plates, to less than 1% of total pressure drop for the other plates.

In the case of 0° plates, no correction was necessary since pressure taps were located on the test plate: in the trough of a furrow and in the centre of the plate as well as 100 mm downstream. No measurements could be obtained in the laminar flow regime as the pressure drop signal was too small.

2.3. *Procedure*

Before the experiments the electrodes were cleaned by polishing them with optical-grade abrasive powder and washing them with carbon tetrachloride. The electrodes were then activated cathodically by hydrogen evolution at a current density of 200 A m^{-2} for 20 min in a solution containing potassium carbonate only.

The electrolyte solutions contained approximately 1.5 M K_2CO_3 and 0.001–0.003 M potassium ferricyanide; ferrocyanide concentrations three times in excess of the ferricyanide ensured that the cathodic reaction was rate-limiting. Fresh solutions were made up daily and the ferricyanide concentration checked by iodometric titration with thiosulphate. Solution densities and viscosities were determined with pycnometers and an Ubbelohde viscometer, respectively.

Nitrogen was bubbled continuously through the reservoir tank to remove any dissolved oxygen. The experiments were performed in a dark-room to prevent the light-catalysed decomposition of ferricyanide.

Voltage scans were made before each set of runs to determine the extent of the limiting current plateau. A potential in the midrange of the current plateaus was then applied to all the experiments in the particular run.

3. RESULTS AND DISCUSSION

The characteristic length dimension (equivalent diameter) was defined as the maximum passage gap. The concept of a hydraulic diameter is applicable only for estimating transfer for the two-dimensional sine duct, from transfer analogies. Table 1 gives characteristic dimensions of the plate patterns chosen.

The experimental results are presented in Figs. 3–6 in the form of friction factors or Colburn j-factor vs Reynolds number. Empirical correlations (for $\beta > 0°$) obtained by least-squares methods are given in Tables 2 and 3. Standard deviations from the experimental data were less than 5 and 7% for the Colburn j-factor and friction factor, respectively. The (heat) transfer data are based on the projected rather than the developed transfer surface area. Transfer data were obtained from measurements done with the central cathode only.

3.2. *Parallel corrugations* ($\beta = 0$): *sine ducts*

Fully developed laminar flow through a sine duct can be analysed mathematically. The friction factor is obtained by solving Poisson's equation (Appendix A). Then, using Lévêque's approximation, the entrance

Table 1. Characteristic dimensions

Sinusoidal corrugation	Amplitude	2.50×10^{-3} m
	Pitch	0.010 m
Plate heat exchanger flow passages $0 \leqslant \beta \leqslant 90°$	Equivalent diameter	0.010 m
	Electrode length	0.112 m
	Cross-sectional free flow area	0.50×10^{-3} m^2
	Projected transfer area	0.0112 m^2
	Ratio of developed to projected area	1.464
Sine ducts $\beta = 0$	Cross-sectional area, each	50×10^{-6} m^2
	Circumference, each	0.02927 m
	Hydraulic diameter	6.83×10^{-3} m
	Number of ducts in parallel	10

region heat transfer is estimated (Appendix B). The resulting equation is converted to the plate heat exchanger conventions (Appendix C). This correlation [equation (16)] has been plotted in Fig. 4(a) for an entrance length of 0.112 m, which corresponds to the electrode length. The experimental data fall slightly below the theoretical curve but show a similar trend.

For high Prandtl (Schmidt) numbers, the turbulent transfer rate is estimated from the friction factor and the asymptotic form of the conventional transfer analogy (Appendix D). The resulting equation (17) is also plotted in Fig. 4(a). The experimental results fall approx. 4% below this semi-theoretical correlation.

3.2. *Effect of corrugation inclination angle*

The effect of the corrugation inclination angle to the main flow direction, β, on thermohydraulic performance is highlighted in Figs. 5 and 6. The main features

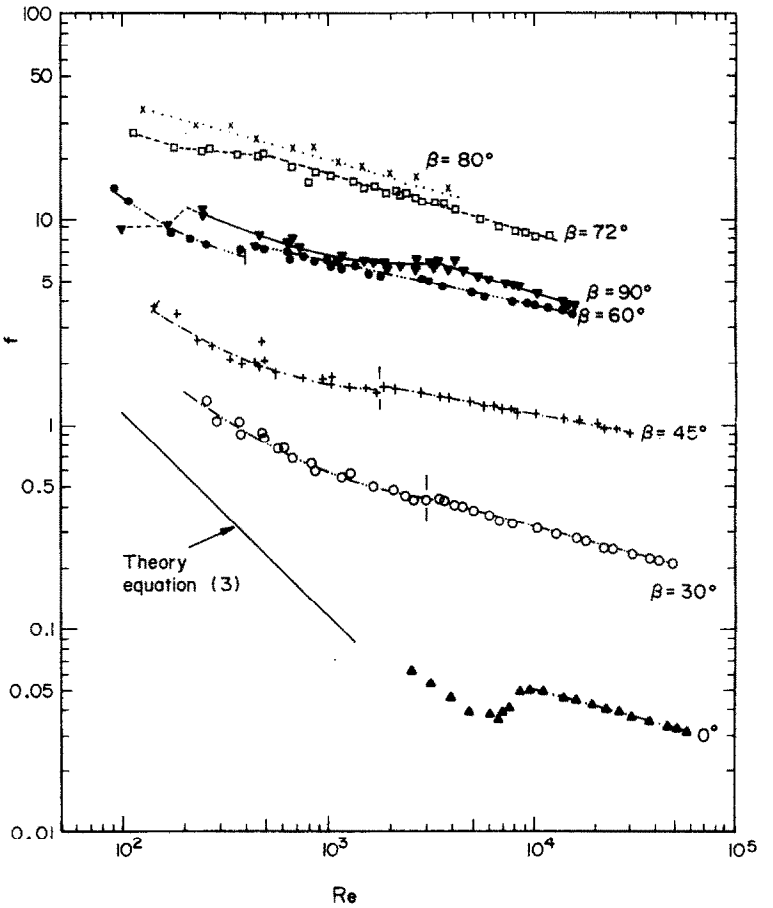

FIG. 3. Experimental friction factors

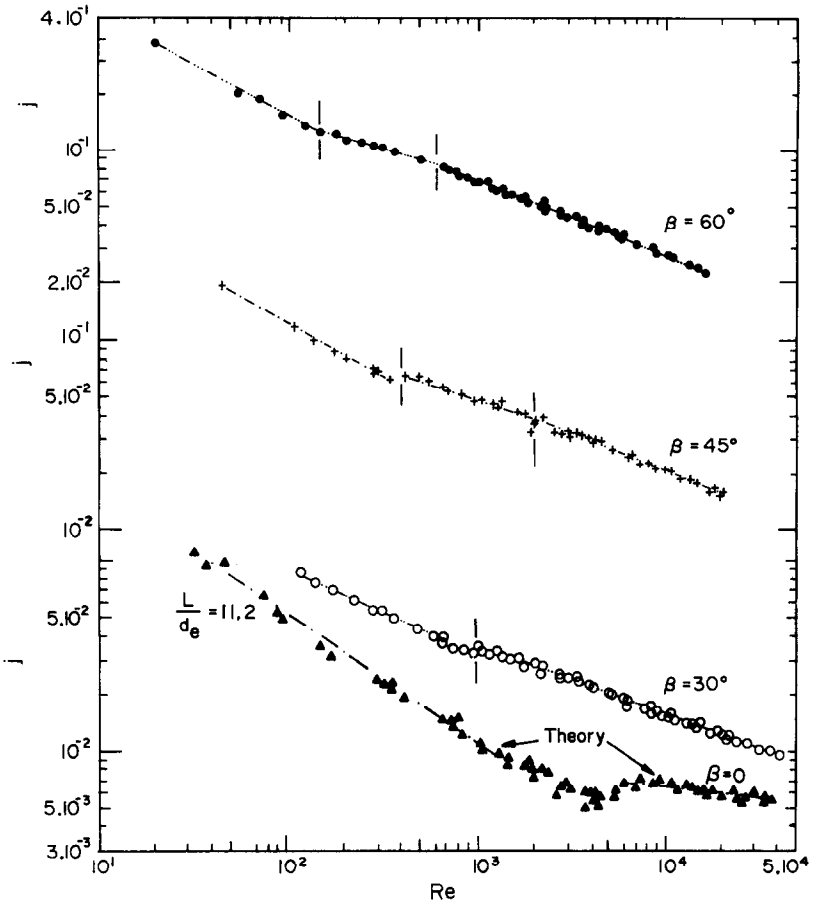

FIG. 4(a). Colburn j-factors.

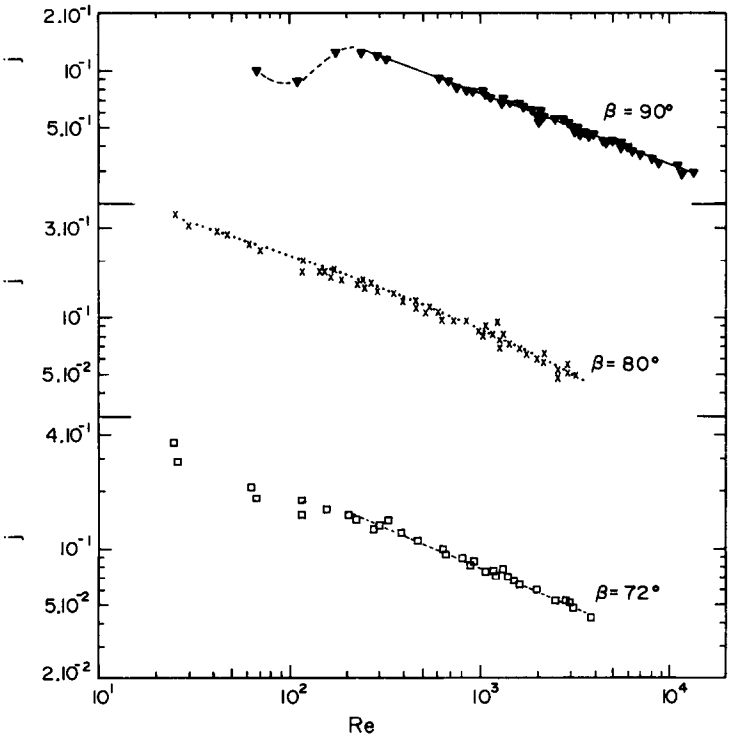

FIG. 4(b). Colburn j-factors.

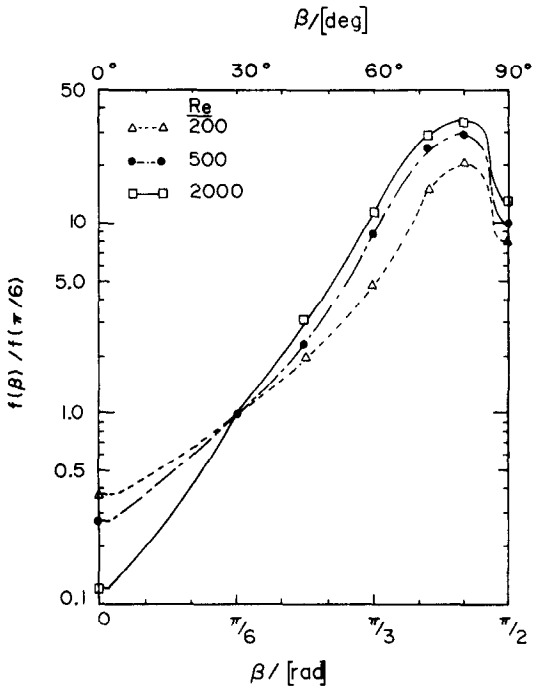

FIG. 5. The effect of the corrugation inclination angle on pressure drop at constant Reynolds number.

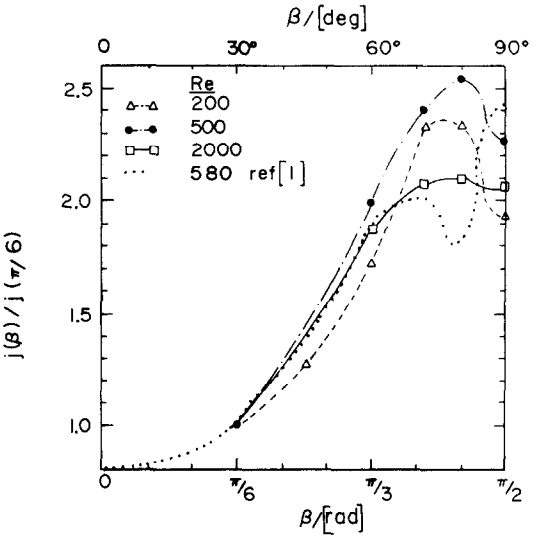

FIG. 6. The effect of the corrugation inclination angle on heat (mass) transfer at constant Reynolds number.

of the curves (obtained in the present study) for pressure drop and transfer at constant Reynolds number are:

—increase with β at an increasing rate up to $\beta \simeq 60°$,
—increase at a decreasing rate for $\beta \simeq 60°$ to $\beta \simeq 80°$,
—maximum at $\beta \simeq 80°$,
—local minimum at $\beta = 90°$.

Symmetry considerations require that the derivatives of the j-factor and friction factor with respect to β should be zero [1] for $\beta = 0°$ and $\beta = 90°$.

The present findings for heat (mass) transfer are at variance with those of Rosenblad and Kullendorff [1]; one of their experimental curves is also shown in Fig. 6. These investigators observed a local maximum at $\beta \simeq 72°$, a local minimum at $\beta \simeq 80°$ and an overall maximum at $\beta = 90°$. They also used sine-wave patterns with a pitch of 10 mm, but in their case the amplitude was 1.6 mm instead of 2.5 mm. This may account for the discrepancy for angles $\beta > 60°$. Alternatively, the corrugations on their plates could have been out of phase with each other for β close to 90°.

3.3. *Flow patterns*

The flow patterns observed in plates with $\beta = 45°$, 80°, and 90° during an independent flow visualization study [7] are shown schematically in Fig. 7. The most important findings were:

$\beta = 90°$. When the plates are assembled with the corrugations perpendicular to the flow direction, flow separation occurs at a Reynolds number of approx. 20.

Table 2. Friction factor correlations

Corrugation angle, β (degrees)	Re-Range	f-Correlation	
0	Laminar (theory*)	$114.4/Re$	(3)
	$8000 < Re < 56000$	$0.552\,Re^{-0.263}$	(4)
30	$260 < Re < 3000$	$0.37+230/Re$	(5)
	$3000 < Re < 50000$	$3.59\,Re^{-0.263}$	(6)
45	$150 < Re < 1800$	$1.21+367/Re$	(7)
	$1800 < Re < 30000$	$5.84\,Re^{-0.177}$	(8)
60	$90 < Re < 400$	$5.03+755/Re$	(9)
	$400 < Re < 16000$	$26.8\,Re^{-0.209}$	(10)
72	$110 < Re < 500$	$19.0+764/Re$	(11)
	$500 < Re < 12000$	$132\,Re^{-0.296}$	(12)
80	$130 < Re < 3700$	$140\,Re^{-0.28}$	(13)
90	$200 < Re < 3000$	$5.63+1280/Re$	(14)
	$3000 < Re < 16000$	$63.8\,Re^{-0.289}$	(15)

* This correlation was obtained by combining equations (A1) and (A3) and equation (A16).

Table 3. Colburn j-factor correlations

Corrugation angle, β (degrees)	Re-Range	j-Correlation		
0	$35 < Re < 800$	$2.53(d_e/L)^{1/3}Re^{-2/3}$	(16)	theory*
	$7000 < Re < 35\,000$	$0.021\ Re^{-0.132}$	(17)	theory*
30	$120 < Re < 1000$	$0.77\ Re^{-0.46}$	(18)	
	$1000 < Re < 42\,000$	$0.44\ Re^{-0.36}$	(19)	
45	$45 < Re < 300$	$1.67\ Re^{-0.56}$	(20)	
	$300 < Re < 2000$	$0.405\ Re^{-0.30}$	(21)	
	$2000 < Re < 20\,000$	$0.84\ Re^{-0.40}$	(22)	
60	$20 < Re < 150$	$1.89\ Re^{-0.54}$	(23)	
	$150 < Re < 600$	$0.57\ Re^{-0.30}$	(24)	
	$600 < Re < 16\,000$	$1.12\ Re^{-0.40}$	(25)	
72	$200 < Re < 4000$	$1.45\ Re^{-0.42}$	(26)	
80	$27 < Re < 500$	$1.05\ Re^{-0.36}$	(27)	
	$500 < Re < 2800$	$1.98\ Re^{-0.46}$	(28)	
90	$300 < Re < 14\,000$	$0.98\ Re^{-0.37}$	(29)	

*Equations (16) and (17) are the same as equations (A8) and (A21), respectively.

With increasing Reynolds number the separated regions grow in size until they fill the major part of the furrows. At $Re \simeq 200$ the free shear layers become unstable and at higher Reynolds numbers the main flow becomes turbulent.

$\beta = 45°$. The fluid flows predominantly along the furrows, i.e. between the corrugations on each of the plates. On reaching the plate edge the fluid streams are 'reflected' and return to the opposite plate edge along the furrows on the opposite side.

Flow patterns similar to those of $\beta = 45°$ are expected for any β in the range up to about 60° (72°?). The essential feature of the flow for these angles is the two sets of criss-crossing streams which induce secondary swirling motions in the flow along the furrows. The driving force that produces swirl in a furrow is the velocity component of the fluid moving along the opposite furrows in a direction perpendicular to the furrow. It is therefore proportional to:

$$\bar{u}_c \sin(2\beta) = 2\bar{u}_c \sin\beta \cos\beta \qquad (30)$$

and is at a maximum when $\beta = 45°$. For angles below $\beta = 45°$, the interaction between the fluid streams is positive, i.e. each of the crossing streams has a velocity component in the same direction as the stream it crosses. For $\beta > 45°$, the interaction is negative in the sense that crossing streams have a retarding effect on each other owing to their velocity components being in opposite directions. We speculate that this retarding effect, which increases with β, eventually leads to the change in flow pattern observed for $\beta = 80°$.

$\beta = 80°$. The fluid still flows mainly along the furrows

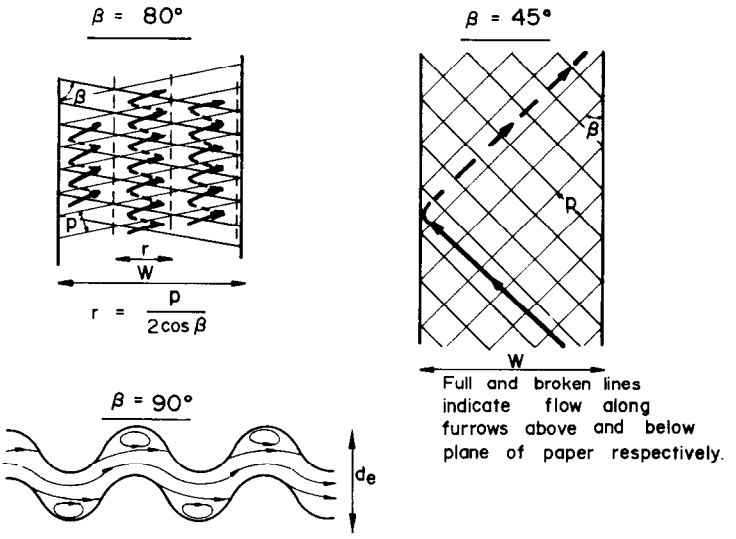

FIG. 7. Bulk flow patterns in plate heat exchanger geometries.

but 'reflection' occurs between plate contact points (see Fig. 7). The flow forms zig-zag patterns in parallel.

The complex interactions between fluid streams lead to early transition to turbulence. The basic flow structures appear to persist even in turbulent flow.

3.4. *Interpretation of transfer data in terms of flow patterns*

$\beta = 90°$. Heat (mass) transfer at Reynolds numbers below 300 is relatively low since the laminar free shear layers of the separated regions are an additional resistance. Transfer across turbulent-free shear layers is, however, usually very effective owing to the absence of a restraining effect such as a solid wall. The additional resistance is therefore effectively removed when the free shear layers become turbulent and there is a sudden increase in heat (mass) transfer [see Fig. 4(b)]. A similar sharp increase in the friction factor is observed at $Re \sim 200$.

The friction factor plot suggests that fully turbulent flow is established only at $Re \sim 3000$ (see Fig. 3), but for heat (mass) transfer effectively turbulent conditions prevail above $Re \sim 300$.

Intermediate angles. It is demonstrated in Appendix E that the secondary swirling motions induced by the streams criss-crossing along the furrows are the main determinant in heat (mass) transfer. At constant plate Reynolds number the velocity of the flow along a furrow is proportional to $1/\cos\beta$ (Appendix C). The effective driving force that produces swirl at constant plate Reynolds number is therefore proportional to $\sin\beta$ for $30 \leqslant \beta \leqslant 72$ [see equation (30)]. The transfer curve at constant plate Reynolds number then flattens above $\beta = 60°$ in accordance with the attenuation of the driving force, as shown in the experimental results in Fig. 6.

An important implication of the transfer being determined by the secondary motions is that plate width is of minor importance for average heat transfer coefficients. This means that zig-zag corrugated patterns (multiple chevrons in parallel) are not expected to produce significant increases in heat transfer coefficients compared with plates having corrugations running their full width. The former could, however, lead to higher pressure drops owing to the increased number of turns the flow has to make.

4. CONCLUSIONS

The corrugation inclination angle, β, is a major parameter influencing the performance of plate heat exchangers: this is because a change in β affects the basic flow structure which is the primary factor influencing pressure drop and heat transfer. Increasing β (at constant Reynolds number) from 0° to 80° leads to pressure drop increases of over $2\frac{1}{2}$ orders of magnitude, although heat transfer increases by a factor of only 4–10. The flow patterns found for various values of β are:

$\beta = 0°$. Two-dimensional channel flow for which transfer rates can be estimated from pressure drop data using conventional transfer analogies.

$30° \lesssim \beta \lesssim 60°$. Sets of criss-crossing streams flowing along the furrows on either side of the flow passage inducing secondary swirling motions; these determine the heat transfer enhancement process.

$\beta = 80°$. Flow consisting of parallel zig-zag patterns; pressure drop and heat transfer are about at their maximum but only marginally higher than for $\beta = 72°$.

$\beta = 90°$. Separated flow regions causing heat transfer and pressure drop to be considerably lower and of approximately the same magnitude as for $\beta = 60°$.

Experimental results obtained for plates with $\beta = 45°$ indicate that transfer rates are almost uniform across the plate width. Pitch-averaged transfer rates are also independent of plate length.

REFERENCES

1. G. Rosenblad and A. Kullendorff, Estimating heat transfer rates from mass transfer studies on plate heat exchanger surfaces, *Wärme-u. Stoffübertr.* **8,** 187–191 (1975).
2. K. Okada, M. Ono, T. Tomimura, T. Okuma, H. Konno and S. Ohtani, Design and heat transfer characteristics of new plate heat exchanger, *Heat Transfer Jap. Res.* **1,** 90–95 (1972).
3. A. F. Savostin and A. M. Tikhonov, Investigation of plate-type heating surfaces, *Teploénergetika* **17,** 75–78 (1970).
4. J. R. Selman and C. W. Tobias, Mass transfer measurements by the limiting current technique, *Adv. chem. Engng* **10,** 211–318 (1978).
5. F. P. Berger and A. Ziai, Optimization of experimental conditions for electrochemical mass transfer measurements, *Chem. Engng Res. Dev.* **61,** 377–382 (1983).
6. M. Baan Hofman, The diffusion coefficients of ferri- and ferrocyanide ions in the presence of potassium carbonate as supporting electrolyte, CERG Memo 81/15, CSIR, Pretoria (1981).
7. W. W. Focke and P. G. Knibbe, Flow visualization in flat ducts with corrugated walls using an electrode-activated pH-indicator. Submitted for publication.
8. International Mathematical and Statistical Libraries, Program TWODEPEP (5th edn), IMSLTDP-0005, Houston, Texas (1983).
9. R. K. Shah, Laminar flow friction and forced convection in ducts of arbitrary geometry, *Int. J. Heat Mass Transfer* **18,** 849–862 (1975).
10. M. A. Lévêque, Les lois de la transmission de chaleur par convection, *Annls Mines Mem.*, Ser. 12, **13,** 201–415 (1928).
11. B. S. Petukhov and V. N. Popov, Theoretical calculation of heat exchange and frictional resistance in turbulent flow in tubes of an incompressible fluid with variable physical properties. *Trans. High Temp.* **1,** 69–83 (1963).
12. S. W. Churchill, Comprehensive correlating equations for heat, mass and momentum transfer in fully developed flow in smooth tubes, *Ind. Engng Chem. Fundam.* **16,** 109–115 (1977).
13. O. T. Hanna and O. C. Sandall, Developed turbulent transport in ducts for large Prandtl or Schmidt numbers, *A.I.Ch.E. Jl* **18,** 527–533 (1972).

APPENDIX A: FRICTION FACTOR FOR FULLY-DEVELOPED LAMINAR FLOW IN A SINE DUCT.

The friction factor for fully-developed laminar flow in a two-dimensional duct is best evaluated from the geometric

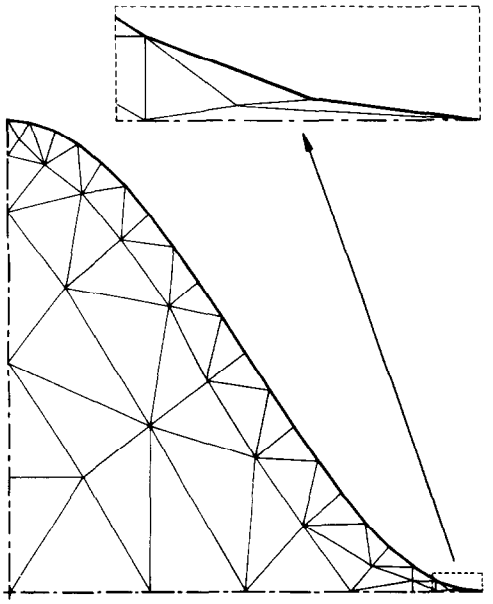

FIG. A1. Finite elements used for sine duct.

constant

$$K = fRe = -2cd_h^2/\bar{u}, \quad \text{(A1)}$$

obtained by solving Poisson's equation

$$\frac{\partial^2 u}{\partial x^2} + \frac{\partial^2 u}{\partial y^2} = \frac{1}{\eta}\frac{dP}{dx} = c \text{ (constant)}. \quad \text{(A2)}$$

From symmetry considerations, it is sufficient to calculate the average flux through one quarter of the sine duct. The curved perimeter was broken into short straight-line segments and the internal region divided into 57 triangular finite elements, as shown in Fig. A1. Equation A2 was then solved numerically (with $c = -1$) using quadratic base functions with the aid of a finite element program [8] and the integral of u evaluated numerically. From this a value for the geometric constant K was obtained:

$$K = 53.3934. \quad \text{(A3)}$$

As a check on the method, the same procedure was applied to the half-sine duct: a sine wave section bounded from below by a flat surface. The only change made to the computer program was to replace the Neumann boundary condition ($\partial u/\partial y = 0$) on the bottom boundary by a Dirichlet condition ($u = 0$). This case was previously analysed by Shah [9] and the geometric factor of $K = 44.875$ evaluated here agreed to within 0.1% with the value quoted by Shah [9].

APPENDIX B: ENTRANCE REGION HEAT (MASS) TRANSFER IN LAMINAR FLOW IN A SINE DUCT

The asymptotic Lévêque model [10] assumes a linear velocity profile inside the concentration boundary layer

$$k = 0.8075\,(D^2\bar{s}/L)^{1/2}. \quad \text{(A4)}$$

Although derived for planar flow with a constant wall velocity gradient, the model can be applied to the present duct geometry provided the temperature (concentration) boundary-layer thickness is very small compared with the radius of wall curvature. This will be the case for short transfer lengths and high Prandtl (Schmidt) numbers.

Expressing the average wall velocity gradient ($\bar{s}$) in terms of the geometric constant K

$$\bar{s} = (KRe/8)(v/d_h^2) \quad \text{(A5)}$$

gives, on substitution into equation (A4) and after some rearrangement

$$Sh_c = 0.40375(K\,Re_c Sc d_h/L)^{1/2}. \quad \text{(A6)}$$

This equation can be rewritten in terms of a Colburn j-factor for the corresponding plate heat exchanger flow passage (see Appendix C)

$$j = 0.40375(A_d/A_p)(Kd_e/d_h)^{1/2}\,Re^{-2/3}(d_e/L)^{1/2}. \quad \text{(A7)}$$

Inserting the numerical values for the dimensions of the sine duct and the plate heat exchanger channel gives

$$j = 2.53(d_e/L)^{1/3}\,Re^{-2/3}. \quad \text{(A8)}$$

APPENDIX C: RELATIONSHIP BETWEEN PLATE AND SUBCHANNEL QUANTITIES

Consider the subchannels (furrows) on one side of the flow channel. The number of subchannels extending over the width of the flow passage is approx.

$$n = (W\cos\beta)/p. \quad \text{(A9)}$$

We assume that fluid always flows parallel to the furrows. The volumetric flow rate along each subchannel is

$$q_c = q/2n = (qp)/(2W\cos\beta). \quad \text{(A10)}$$

The cross-sectional free flow area for the plate heat exchanger passage is

$$A = Wd_e/2 \quad \text{(A11)}$$

and for a subchannel it is

$$A_c = pd_e/4. \quad \text{(A12)}$$

The superficial velocity in each subchannel is therefore

$$\bar{u}_c = q_c/A_c = 2q/(Wd_e\cos\beta). \quad \text{(A13)}$$

The relationship between subchannel and plate Reynolds number follows from equations (A11) and (A13)

$$Re_c = [d_h/(d_e\cos\beta)]\,Re_p. \quad \text{(A14)}$$

The average channel Sherwood number can also be expressed in terms of the plate Sherwood number

$$Sh_c = (d_h/d_e)(A_p/A_d)Sh_p. \quad \text{(A15)}$$

The above results apply to the case $\beta = 0$ even when the subchannel is taken to be the sine duct instead of a furrow (one-half of the sine duct). For this special case we also require relationships between the plate and channel/duct friction factors and Colburn j-factors. These are given by

$$f_c = (d_h/d_e)^2 f \quad \text{(A16)}$$

$$j_c = (d_h/d_e)j. \quad \text{(A17)}$$

APPENDIX D: ESTIMATING TURBULENT HEAT (MASS) TRANSFER FROM FRICTION FACTOR DATA FOR THE SINE DUCT

The asymptotic form, at high Prandtl (Schmidt) numbers, of the conventional transfer analogy [11] is

$$j \sim B\sqrt{f}. \quad \text{(A18)}$$

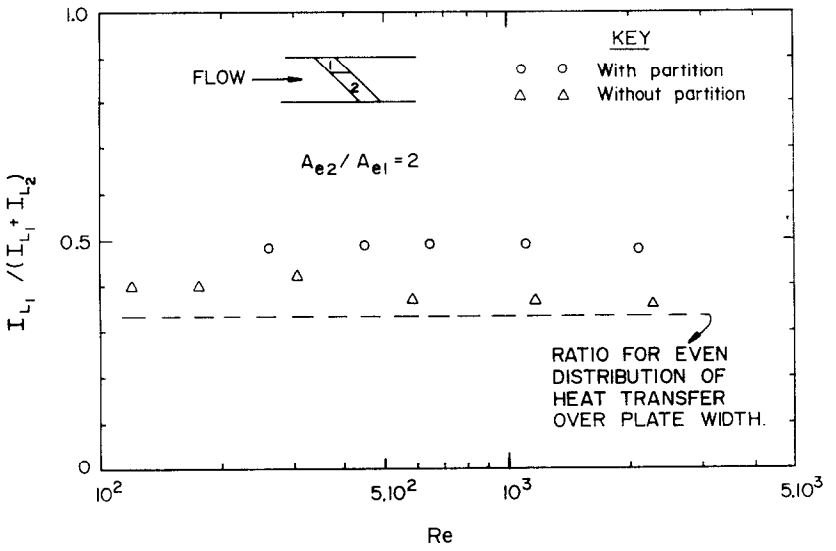

FIG. A2. Transfer to a segmented electrode with and without a partition between test plates with $\beta = 45°$.

For heat transfer in tubes at high Prandtl numbers Churchill [12] proposed

$$j = 0.0157\, Re^{-0.125}. \tag{A19}$$

This equation is in good agreement with the results obtained by other investigators [12, 13]. By substituting the Blasius friction factor correlation for tubes

$$f = 0.3164\, Re^{-0.25}. \tag{A20}$$

into equation (A18), a value for $B = 0.0279$ is deduced from equation (A19).

Assuming now that equation (A18), with $B = 0.0279$, is also valid for channels other than those of circular cross-section, one obtains for the sine duct (on inserting the experimental friction factor correlation)

$$j = 0.021\, Re^{-0.132} \tag{A21}$$

APPENDIX E: THE FEATURE OF THE FLOW THAT DETERMINES HEAT (MASS) TRANSFER ENHANCEMENT

Flow visualization studies [7] on plates with $\beta = 45°$ have shown that:

—the fluid flows along the furrows on either side of the passage, from edge to edge; and
—the two sets of criss-crossing fluid streams induce secondary swirling motions in the flow along the furrows.

It is of interest to determine which, if either, of these two main features of the flow determines the heat transfer enhancement process. For flow along a short path length, entrance region conditions are expected because the boundary layers are still developing. In this case, higher transfer rates are expected in the upstream parts of the furrows. However, a swirling motion of sufficient strength could lead to a more uniform transfer rate across the plate width.

Additional experiments were done with plates ($\beta = 45°$) containing a segmented graphite cathode. The cathode shape was a parallelogram. It extended over the width of the plate with the electrode edges running parallel to the corrugation crests. It covered three adjacent furrows from crest to crest. A gap of 1 mm running parallel to the cell axis divided the electrode into two parts covering $\frac{1}{3}$ and $\frac{2}{3}$ of the electrode area respectively.

Overall heat (mass) transfer rates measured with the combined electrodes were in agreement with the results obtained for nickel-plated brass electrodes presented in the main text. This result suggests that pitch-averaged heat transfer coefficients are uniform across the plate length.

The results obtained when the smaller electrode segment was placed on the upstream side are presented in Fig. A2 as the ratio of smaller-segment current to total current. No significant variation of this ratio with Reynolds number is observed. Since the current ratios are slightly above the value of $\frac{1}{3}$ (which would indicate an even current distribution), a small edge effect is indeed present.

The unsymmetrical partitioning of the electrode allows measurements to be made with two different geometric arrangements, i.e. smaller electrode segment downstream or upstream. With data for these two arrangements it is possible to estimate the magnitude of the edge effects at both edges, provided that it can be assumed that these edge effects are limited to a distance that is shorter than the length of the smaller segment. Based on this assumption, the incremental contributions of upstream and downstream edge effects are 5 and 2%, respectively at $Re \sim 2000$. These low values suggest that the secondary swirling motion is the main determinant in the heat transfer enhancement process. The small deviations may well represent the effect of the turning of the flow at the edges.

As a further check, the experiments were repeated under conditions in which the interaction between the two sets of fluid streams was effectively eliminated. This was achieved by inserting a rigid celluloid sheet ~0.1 mm thick and 70 mm wide between the test plates. This left 15 mm open on each side of the passage to allow the fluid streams to turn. Current ratios measured for this case are also shown in Fig. A2 and a marked increase in the upstream edge (or entrance) effect is indicated. The smaller electrode segment registered roughly the same current as the downstream segment which had twice the area. Estimated positive edge effects for $Re \sim 2000$ are 29 and 10%, respectively for the upstream and downstream parts. In addition, overall transfer decreased to 65% of the value for plates without a partition. These observations confirm the dominant role of the secondary motion resulting from fluid stream interactions.

L'EFFET DE L'ANGLE D'INCLINAISON DES CORRUGATIONS SUR LA PERFORMANCE THERMODYNAMANIQUE D'ECHANGEURS DE CHALEUR A PLAQUES

Résumé—L'angle d'inclinaison entre les corrugations et la direction générale de l'écoulement représente un paramètre important dans la performance thermodynamique d'un échangeur de chaleur à plaques. L'application d'une technique améliorée pour la visualisation de l'écoulement a démontré qu'à des angles jusqu'à 80° le liquide coule essentiellement le long des corrugations dans chaque plaque. Un tourbillon secondaire est imposé sur l'écoulement le long d'une corrugation par l'interaction avec des écoulements le long de la paroi opposée. L'application de l'analogie électrochimique du transfert de matière prouve que ce tourbillon secondaire détermine le processus de transfert ; comme conséquence de ce mouvement il résulte une distribution assez équilibrée du transfert sur la largeur des plaques. Le maximum de la vitesse de transfert observé à un angle d'environ 80° est expliqué à base du profil de l'écoulement. A des angles plus élevés le profil de l'écoulement devient moins efficace pour le transfert; en particulier à un angle de 90° il résulte une nette séparation de l'écoulement.

EINFLUSS DER PLATTENWELLENNEIGUNGSWINKEL AUF DIE THERMODINAMISCHEN LEISTUNG EINES PLATTENWÄRME-AUSTAUSCHERS

Zusammenfassung—Der Neigungswinkel zwischen Plattenwellen und der allgemeinen Fliessrichtung ist ein wichtiger Parameter in der thermodynamischen Leistung eines Plattenwärme-austauschers. Die Anwendung einer verbesserten Technik der Sichtbarmachung der Fliessbewegung hat bewiesen, dass bei Winkeln bis 80° die Flüssigkeit grösstenteils längs der Furchen an jeder Platte fliesst. Die Strömung längs einer Furche erfährt eine sekundäre Wirbelbewegung durch die querlaufenden Strömungen längs der entgegengesetzten Wand. Die Anwendung der elektrochemischen Massenübertragungsanalogie liefert den Beweis, dass diese sekundäre Wirbelbewegung den Übertragungsprozess bestimmt ; als Konsequenz dieser Bewegung wird eine ziemlich gleichmässige Verteilung der Übertragung über die Breite der Platte erreicht. Das beobachtete Maximum der Übertragungsgeschwindigkeit bei einem Winkel von ungefähr 80° wird durch das beobachtete Fliessprofil erklärt. Bei höheren Winkeln wird das Fliessprofil weniger effektiv für die Übertragung; im einzelnen erscheint bei 90° eine klar sichtbare Trennung des Flusses.

ВЛИЯНИЕ УГЛА НАКЛОНА ВЫСТУПА НА ГИДРАВЛИЧЕСКИЕ ХАРАКТЕРИСТИКИ ПЛАСТИНЧАТЫХ ТЕПЛООБМЕННИКОВ

Аннотация—Установлено, что угол наклона между выступами пластин и направлением потока является основным термогидравлическим параметром пластинчатых теплообменников. Применение усовершенствованного метода визуализации течения показало, что при углах вплоть до 80° жидкость движется в основном вдоль выемок на каждой пластине. Вторичное закрученное движение налагается на течение вдоль выемки в том случае, когда направление движения пересекается потоками, движущимися вдоль выемок на противоположной стенке. С помощью электрохимической аналогии массопереноса показано, что это вторичное движение определяет процесс переноса: как следствие этого движения перенос почти однородно распределяется поперек ширины пластин. Полученная максимальная скорость теплопереноса при углах около 80° объясняется наблюдаемой картиной обтекания. При больших углах обтекания структура течения меньше влияет на процесс переноса, в частности, при 90° наблюдается заметный отрыв потока.